International Journal of Nanomedicine Dovepress

Open Access Full Text Article ORIGINAL RESEARCH

Stealth-Engineered Albumin-Coated Nanoparticles for Targeted Therapy: Effective Drug Delivery and Tumor Suppression in Xenograft-Zebrafish Model

Sara Bozzer[1], Maria Cristina Grimaldi[1], Luca De Maso[1], Marcello Manfredi[2], Giuseppe Toffoli[3], Michele Dal Bo[3], Daniele Sblattero[1], Paolo Macor[1]

[1]Department of Life Sciences, University of Trieste, Trieste, 34127, Italy; [2]Department of Translational Medicine, Center for Translational Research on Autoimmune and Allergic Diseases, CAAD, University of Piemonte Orientale, Novara, Italy; [3]Experimental and Clinical Pharmacology Unit, C.R.O.-IRCCS, Aviano, 33081, Italy

Correspondence: Paolo Macor, Email pmacor@units.it

Purpose: In the bloodstream, nanoparticles (NPs) interact with serum proteins to form the protein corona, which includes both opsonins, promoting NP recognition and elimination, and dysopsonins, which can inhibit opsonin activity. Albumin, the most abundant serum protein, is part of this corona and can act as a dysopsonin, potentially hiding NPs from the immune system. This study aims to investigate how a covalently bound layer of human serum albumin (HSA) on polymeric NPs affects the protein corona and their behavior in the immune system.

Methods: We covalently attached HSA to the surface of polymeric NPs to modify the protein corona composition. These HSA-covered nanostructures were then decorated with an anti-CD19 recombinant antibody fragment to target malignant B cells, specifically acute lymphoblastic leukemia (ALL) cells. The safety profile and bioavailability of these targeted HSA-nanoparticles were evaluated in vitro and in vivo using a human-zebrafish xenograft model of ALL. The efficacy of the nanostructures in delivering encapsulated doxorubicin and suppressing tumor growth was also assessed.

Results: The HSA coating on polymeric NPs effectively modified the protein corona, preventing opsonization and subsequent macrophage-mediated elimination. The targeted HSA-nanoparticles maintained a safe profile with reduced macrophage interaction and specifically targeted tumor cells in the xenograft model. This resulted in the successful delivery of doxorubicin, tumor growth suppression, and increased survival of the model organisms.

Conclusion: The study demonstrates that HSA-coated nanoparticles can be used as a therapeutic nanoplatform with a safe profile and enhanced bioavailability. The ability to decorate these nanostructures with specific targeting agents, such as anti-CD19 antibodies, opens up the potential for developing versatile therapeutic platforms that can be tailored to target various clinical conditions.

Keywords: polymeric nanoparticles, targeting antibody, protein corona, albumin, drug delivery, xenograft model

Introduction

Nanoparticles (NPs) are gaining increasing interest in the medical field due to their intrinsic and extrinsic properties.[1–3] Among the various NPs available, synthetic polymers that are both biodegradable and biocompatible hold significant promise for nanocarrier development. This is attributed to their chemical versatility, high purity, and the controlled manufacturing processes they offer, which surpass those of natural materials.[4] In particular, polylactide-co-glycolic acid (PLGA) is a copolymer composed of poly(glycolic acid) and poly(lactic acid) linked by ester bonds, resulting in a linear, amorphous aliphatic polyester structure that has been approved by the US Food and Drug Administration and European Medicines Agency as delivery systems for therapeutic agents.[5] Biocompatibility is one of the features that support the success of this delivery system. In vivo, the release of the payload is allowed by the fact that the polymer is degraded by

Received: 12 July 2024
Accepted: 18 October 2024
Published: 10 December 2024

Graphical Abstract

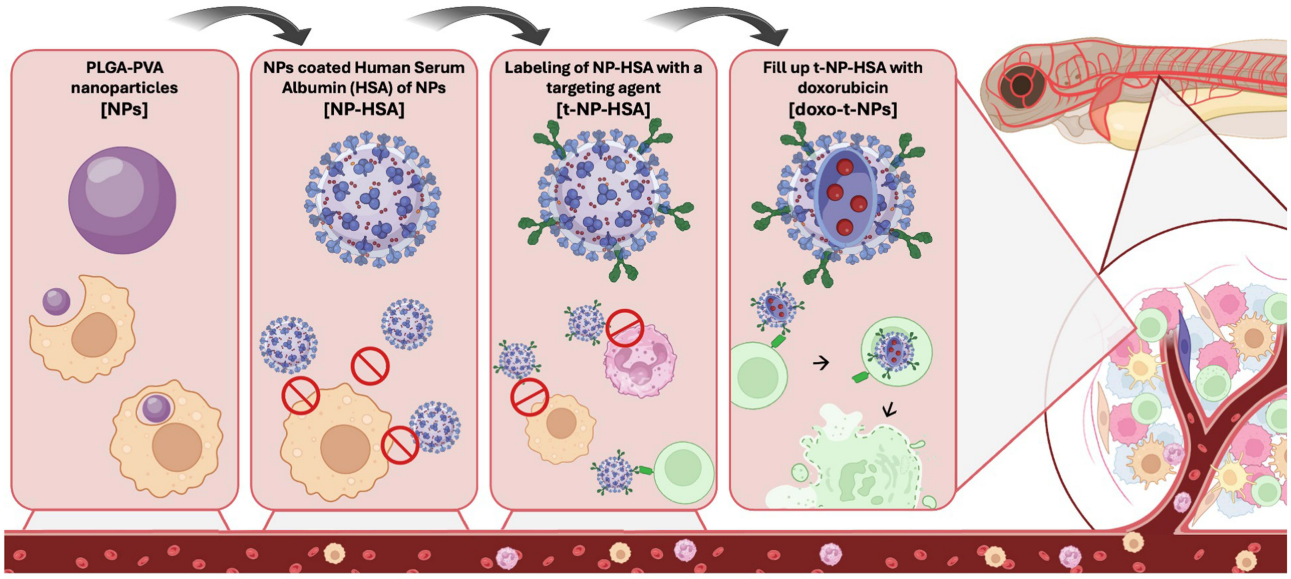

hydrolysis and converted back to the original monomers (ie, lactic acid and glycolic acid), processed through cellular metabolic pathways and excreted as CO_2 and H_2O, resulting in minimal systemic toxicity.[2] PLGA nanostructures are often stabilized by employing poly(vinyl alcohol) (PVA) as an emulsifier, another biodegradable and widely used water-soluble polymer, non-toxic for living tissues.[6]

Nanocarrier composition and size affect the in vivo behavior. Particles larger than 200 nm are quickly recognized as not "self" and eliminated by the mononuclear phagocyte system (MPS) mainly present in the liver, spleen, lung, and inflammatory tissues. It relies on the recognition by a class of serum proteins called opsonins (ie, immunoglobulins, complement components, and coagulation proteins), which target the surfaces of nanocarriers in the context of a 'biomolecular corona' or 'protein corona' and can then be recognized by specific receptors on macrophages of MPS.[2,7–9] Other serum proteins have been documented in the protein corona, including dysopsonins that can prevent the absorption of opsonins, increase the stealth of the NPs, and finally reduce their clearance; examples of dysopsonins are apolipoproteins, regulators of the complement system, and albumin.[8,9]

Several methods were explored to limit NPs elimination by the immune system after opsonization, primarily via surface modifications to enhance the presence of dysopsonin in the protein corona with respect to opsonins.[10,11] The best-known dysopsonin is albumin, the most abundant endogenous plasma protein, which is characterized by high solubility and long half-life in blood and is important for the transport of different molecules in the bloodstream but is also used by many cancer cells to create energy and nutrients.[12,13] All these properties contribute to considering albumin as a promising surface modifier and protective component of the protein corona. Different groups focused on bovine serum albumin (BSA) and demonstrated that a pure albumin corona, surrounding NPs, formed in the absence of competitive adsorption from other proteins, acts as a protective coating for NPs.[12–16] These studies focused on bovine and not human albumin and do not provide details of the changes in protein corona but clearly demonstrated that it inhibits the plasma proteins' adsorption, finally prolonging the circulation time of NPs. Most importantly, the binding of albumin to polymeric NPs depends on low-affinity interactions; this protein is usually reported to be part of the "soft" protein corona, which can be easily replaced by opsonins, as part of the "hard" protein corona, and finally losing the stealthing activity.[17]

In this manuscript, we characterize a new PLGA/PVA platform characterized by a superficial covalent-bound layer of Human Serum Albumin (HSA), aiming to stabilize this dysopsonin on the surface of polymeric NPs, to reduce the presence of opsonins and the consequent elimination by macrophages. The results show the modification of the protein

corona caused by the permanent presence of human albumin and the consequence of decreased elimination through phagocytosis.

This platform was also tested in the development of a targeted drug delivery system for the treatment of B-cell malignancies.

The use of stealth nanocarriers as vehicles for drug transport is an important tool to overcome the toxicity associated with chemotherapeutics, such as off-target effects and systemic toxicity. The association with targeting strategies (both passive or active) or with stimulus-sensitive mechanisms enhances the specificity and, as a consequence, the safety of the approach; in particular, targeting approaches are being developed to specifically deliver material to cancer cells avoiding normal cells. This selectivity is based on the interaction between a tumor-associated/specific antigen on cancer cells and targeting molecules on nanosystems.[18–20] Various classes of targeting agents can direct NPs to specific tissues, including proteins (such as antibodies and their fragments), aptamers, and small molecules like vitamins and peptides. Among these, antibodies (mAbs) and engineered antibodies, such as single-chain variable fragments (scFvs) and antigen-binding fragments (Fabs), are the most frequently utilized due to their high specificity and affinity.[21,22] Cell surface antigens are used to target B-cell malignancies.[23–26] CD20 is an example of a protein, characterizing mature B cells to plasmablasts but not expressed on stem cells, targeted for ablative B-cell therapy;[27–29] however, other B-cell malignancies, characterized by early appearance, are not targeted by anti-CD20, so other antigens are being investigated. CD19, a 95-kDa protein important for B cell signaling, is present almost exclusively on Blymphocytes at nearly all development stages.[30] Current clinical trials for anti-CD19 therapies encompass monoclonal antibodies (mAbs), antibody-drug conjugates (ADCs) targeting cytotoxic drugs, bispecific antibodies, and chimeric antigen receptor (CAR) T-cells.[31,32]

Here, we also report the characterization of a drug-loaded biodegradable NPs functionalized with an anti-CD19 scFv-Fc as a targeting mechanism, aiming to demonstrate that a protective covalently linked layer of HSA limits the recognition by phagocytic cells also in the presence of a surface antibody. This therapeutic approach specifically targets CD19-expressing B cells and results in a prominent drug delivery system that limits drug-related side effects and increases animal survival in a zebrafish xenograft model of B-cell malignancy.

Materials and Methods

Cells Culture and Count

NALM-6 and THP-1 cells (from DSMZ, Germany) were defrosted and then maintained in RPMI-1640 medium (Sigma-Aldrich Co., St Louis, MO, USA) supplemented with 10% fetal bovine serum (FBS, Sigma-Aldrich Co.), 100U/mL penicillin–streptomycin (Sigma-Aldrich Co.) and 1% L-glutamine (Sigma-Aldrich Co.) at 37°C, 5% CO2.

THP-1 cells were differentiated to macrophages incubating cells for 72h with 100ng/mL of Phorbol 12-myristate-13-acetate (PMA, Sigma-Aldrich Co).

The trypan blue exclusion assay was used to count live cells in the Bürker chamber.

Production of the Targeting Mechanism

VH and VL of MOR208 (Patent n°: US 2014/0227277 A1), also known as Tafasitamab and Fc-modified region were used to design a humanized anti-CD19 antibody, then produced as previously described by our group.[33] Briefly, the CHO cell line (ThermoFisher) was transfected with a vector coding for the targeting molecule, cultured to maximize production, purified by protein A affinity chromatography (Sigma-Aldrich Co)., and then quantified.

Production of PLGA-PVA Nanoparticles

As previously published,[33,34] PLGA-PVA-NPs were produced in our laboratory following the Vasir and Labhasetwar protocol.[35] PLGA-PVA-NPs were then coated with HSA (Sigma-Aldrich Co.) or the anti-CD19 scFv-Fc targeting mechanism through the EDC/sulfoNHS Crosslinking protocol (Thermo-Fisher Scientific).

Characterization of Nanodevices

Dynamic Light Scattering (DLS)

NPs were diluted in 0.2µm filtered MilliQ H2O and then analyzed by DLS technique using Zetasizer Nano ZSP (Malvern Panalytical, UK).[33]

Transmission Electron Microscopy (TEM)

As aforementioned,[33] NPs (10µL) were centrifuged for 5 minutes at 5000g and resuspended in 10µL of 0.2µm filtered MilliQ H_2O; samples were then deposited on a copper-coated carbon screen, dried, and analyzed using CM 200 TEM (Philips).

Enzyme-Linked Immunosorbent Assay (ELISA)

As previously described by our group,[33] a sandwich ELISA was set coating anti-HSA antibody (Sigma-Aldrich Co.) and blocking unbound sites. Samples were added for 1 hour and the presence of HSA-coating was revealed through a biotin-conjugated anti-HSA (Sigma-Aldrich Co.) antibody and AP-conjugated streptavidin (Sigma-Aldrich Co). To detect the presence of the anti-CD19 scFv-Fc, an AP-conjugated anti-human secondary antibody (Sigma-Aldrich Co.) was used. Data were presented as OD 405nm.

Western Blot Analysis

Samples were separated by SDS-PAGE and then transferred to a nitrocellulose membrane (GE HealthCare, Chicago, IL, USA) by Western blot. The membrane was then blocked and incubated with a biotin-conjugated anti-HSA antibody and then with AP-conjugated streptavidin. The membrane was developed with BCIP and NBT (Sigma-Aldrich Co.) in alkaline phosphatase (AP) Buffer (Tris-HCl 100mM, NaCl 0,1M, $MgCl_2$ 5mM pH 9.6).

Mass Spectrometry

NPs were incubated with NHS (Normal Human Serum: pooled sera from, at least, 30 healthy donors obtained after written informed consent and after the approval of the formally constituted review board of the ethics committee of our Institution, in accordance with the Declaration of Helsinki), diluted 1:10 in PBS, for 1h, washed trice, and prepared for mass spectrometry analysis, as previously reported.[33] Briefly, proteins were denatured with TFE (Sigma-Aldrich Co.) and then subjected to reduction; digested peptides were then desalted, the sample was vacuum-evaporated, and reconstituted in the mobile phase for analysis.[36] Peptides were analyzed with a UHPLC Vanquish system (ThermoFisher Scientific, Waltham, MA, USA) coupled with an Orbitrap Q-Exactive Plus (ThermoFisher Scientific).

Red Blood Cells Lysis

As previously described by our group,[33] NPs were diluted in Complement Fixation Diluent (CFD, NaCl 142mM, Na-5-5-dietilarbiturato 5mM, $MgCl_2$ 0.5mM, agar 0.05%, NaN_3 0.01%, EGTA 10mM) and incubated with 50µL of sheep erythrocytes for 30 minutes at 37°C. Samples were diluted with 1mL of PBS-EDTA and centrifuged. The OD of the supernatant was analyzed at 415 nm using Infinite M200 (TECAN).

Clotting Test

NPs and NHP (Normal Human Plasma: pooled plasma from, at least, 30 healthy donors obtained after written informed consent and after the approval of the formally constituted review board of the ethics committee of our Institution, in accordance with the Declaration of Helsinki), were seeded in a 96-well plate and $CaCl_2$ 20mM was added to initiate the clotting reaction. The turbidity has been read at 405nm every 2 minutes for 70 minutes using Infinite M200 (TECAN).[33]

CH50 Assay

As previously set up in our laboratory,[33] NHS and NPs were incubated for 2 hours at 37°C. Samples were then centrifuged and the supernatant was analyzed by diluting in CFD and adding IgM-sensitized sheep erythrocytes. After 30 minutes at 37°C, the lysis reaction was stopped with 1mL of PBS-EDTA and centrifuged. The OD of the supernatant was analyzed at 415nm using Infinite M200 (TECAN).

Characterization of Nanodevices

As previously published,[33,34] PLGA-PVA-NPs were produced in our laboratory following the Vasir and Labhasetwar protocol.[35] PLGA-PVA-NPs were then coated with HSA (Sigma-Aldrich Co.) or the antiCD19 scFv-Fc targeting mechanism through the EDC/sulfoNHS Crosslinking protocol (Thermo-Fisher Scientific).

Flow Cytometric Analysis

Binding of Nano-Devices to White Cells

White cells were initially isolated through Ficoll-Paque™ from healthy donors and then macrophages were obtained by consecutive selections of adherent cells, as previously detailed;[33] cells (macrophages or other leukocytes) were incubated, eventually in the presence of NHS (diluted 1:10 in PBS), with NPs or NP-HSA at 37°C for 1 hour and then analyzed by flow cytometry. Lymphocytes were selected during analysis for their dimension and complexity from other leukocytes by Attune® NxT (ThermoFisher Scientific); data were analyzed with Attune NxT Software.

Binding of anti-CD19 scFv-Fc on NALM-6 Cells

Cells were incubated with anti-CD19 scFv-Fc (5ng/μL) or with controls (anti-SV5 antibody, or anti-CD19-PE conjugated antibody - BD Company, NJ, USA) at 37°C for 1 h, as previously described by our group.[33] The binding was then revealed with the secondary AlexaFluor-488 conjugated anti-human antibody (ThermoFisher Scientific) by flow cytometric analysis.

Binding and Internalization of Nano-Devices in Cells

NPs were incubated with NHS (10% of NHS as final concentration) for 15 min and then added to NALM-6 for 1 hour at 37°C. The binding on/internalization in the cells was evaluated by flow cytometric analysis, as previously reported.[33]

Immunofluorescence Analysis

Binding of anti-CD19 scFv-Fc on NALM-6 Cells

Antibody/cell interaction was performed as described for cytofluorimetric analysis. The nuclei were stained with DAPI (Sigma-Aldrich Co.) for 5 minutes. Slides were analyzed using the Nikon Eclipse Ti-E live cell imaging system and images were analyzed using Image-J software.

Binding and Internalization of Nano-Devices in Cells

Antibody/cell interaction was performed as described for cytofluorimetric analysis. Cells were stained with DAPI (nuclei) for 5 minutes, and Vybrant Fast DiI (membranes), and cytocentrifuged on a slide and analyzed using the Nikon Eclipse C1si system and Image-J software.

In vivo Experiments on Zebrafish Embryos

All experimental procedures involving animals were done under Ministerial Approval 04086.N.SGL. Zebrafish eggs were placed in E3 Medium (5mM NaCl, 0.17 mm KCl, 0.33 mm $CaCl_2$, 0.33mM $MgSO_4$, and 0.1% Methylene Blue), incubated at 28°C, and 24 hours after fertilization (hpf) the eggs were manually dechorionated. Embryos were then placed in E3 Medium supplemented with phenylthiourea (PTU, Sigma-Aldrich Co.) to inhibit the production of melanin.

Xenograft Models

As previously published,[33,34] 48 hpf embryos were anesthetized using tricaine. NALM-6 cells were labeled with VybrantTM Fast DiD (Thermo Fisher Scientific) or calcein red-orange AM (calcein-AM, Thermo Fisher Scientific), and ~500 cells/embryo were injected in the duct of Cuvier using Nanoject II Auto-Nanoliter Injector (Drummond Scientific Co., Broomall, PA, USA) using a SteREO Microscope Discovery.V8 (Zeiss, Oberkochen, Germany, UE). Embryos were kept at 30°C and then analyzed using the Nikon Eclipse Ti-E live system and Image-J software.

NPs Biodistribution Studies

NPs biodistribution studies were performed on healthy and tumor-bearing embryos, by injecting NPs (4.6nL/embryo) in the duct of Cuvier of anesthetized embryos using capillary glasses and a Nanoject II Auto-Nanoliter Injector (Drummond Scientific Co).[33,34]

At 24hpi, NP biodistribution was evaluated using the Nikon Eclipse Ti-E live system and analyzed with Image-J software. The fluorescence in the area of interest was then quantified in each larva, and the corrected total cell fluorescence (CTCF) was calculated as follows:

CTCF = IntegratedDensity − [(AreaROI cells) × (MeanFluorescenceBackground)]

Results

Nanoparticles' Shell Characterization

PLGA-PVA NPs were prepared by a double emulsion solvent evaporation method following the protocol of Vasir and Labhasetwar and with minimal modifications. In particular, 2 types of NPs were initially prepared: NP, and NP-HSA (Figure 1). The core of the NPs consists of FITC-conjugated BSA to allow visualization by fluorescence microscopy. PLGA (30mg/mL) and PVA (2% w/v) are solely present in the shell of uncoated in NP, or covalently coated with HSA (7.5mg/mL) in NP-HSA, through EDC/sulphoNHS linker that allows the covalent binding using carboxylic acid on the NPs and the primary amines of the lysine residues in the proteins. The binding of HSA was done to verify the concealment of the NPs to the human immune system and acts like a covalently bound dysopsonin.

PLGA-PVA NPs were initially characterized for their average diameter, zeta potential and polydispersity index (PDI) (Figure 1A). The covalent binding of HSA increases the diameter from 322 to 348 nm, maintaining a similar PDI. Both NPs exhibit a negative surface charge, slightly more evident for uncoated samples (NP, −24.1 mV) than coated NPs (NP-HSA, −14.6 mV), in line with the reduction of polymeric carboxylic groups after the binding with a neutral protein like HSA. The regular round shape of the NPs was verified by electron microscopy analysis (Figures 1B, and C). Transmission Electron Microscopy (TEM) is preferable over Scanning Electron Microscopy for visualizing NPs, particularly PLGA-PVA NPs coated with albumin, due to the higher resolution crucial for observing fine details of the nanoparticle structure. A similar encapsulation efficiency was confirmed in NP and NP-HSA, by exploiting the intrinsic fluorescence of the FITC-BSA (maximum excitation/emission 495/521 nm), as previously described by our group for a similar preparation of NPs. Moreover, HSA, present only on NP-HSA, was detected by both ELISA (Figure 1D) and Western blot analysis (Figure 1E).

The formulations were stably stored at 4°C, for up to 10 months, showing no variation in their physio-chemical characteristics and no aggregation (Figure 1F).

Protein Corona Proteomic Identification

Because the initial hypothesis was that a preformed, covalently bound, albumin corona should protect from nonspecific bindings and reduce the deposition of opsonins, the composition of the protein corona on NP and NP-HSA was deeply characterized by LC-MS/MS and then compared. To this end, both NPs were incubated in NHS for 1h and washed three times to obtain the identification and abundance of adsorbed proteins. HSA decoration significantly affected the protein corona (Figure 2A): a total of 79 proteins were adsorbed on NP and 105 on NP-HSA. Forty-eight proteins were specifically targeted polymeric NP, 74 proteins were bound only on NP-HSA, and finally, 31 proteins are associated with both preparations of NPs (Supplementary Table 1).

In both nanostructures, a relevant part of the identified proteins consists of apolipoproteins and proteins part of the coagulation cascade or the complement system. These molecules represent both opsonins and dysopsonins, enhancing the uptake by MPS preventing the clearance, respectively. Therefore, opsonins and dysopsonins revealed through LC-MS/MS analysis were extracted from supplementary Table 1, and their content was compared between NP and NP-HSA, in order to evidence the effect of covalently bound HSA in final corona composition. The results, summarized in Figure 2B, initially showed that more opsonins are present on the surface of NP-HSA with respect to NP; IgG and IgM can be responsible for the activation of the classical pathway of the complement system and contribute to particle opsonization. This is confirmed by the

A

Name	Structure	Coating agent	Targeting agent	Encapsulated agent	Average Diameter (nm)	Polydispersity Index (PDI)	Zeta potential (mV)
NP		none	none	FITC-BSA (20 mg/mL)	322.4 ± 3.71	0.19 ± 0.02	−24.1 ± 0.55
NP-HSA		HSA (7.5 mg/mL)	none		348.7 ± 4.43	0.18 ± 0.03	−14.6 ± 0.72

B

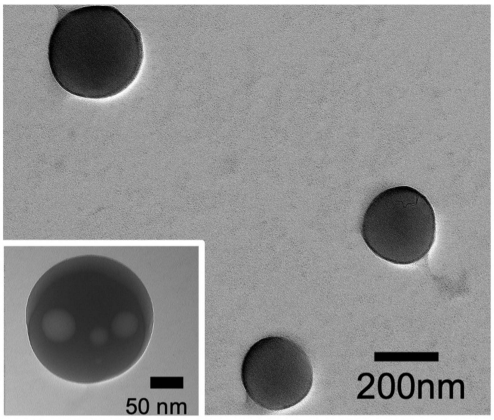

C

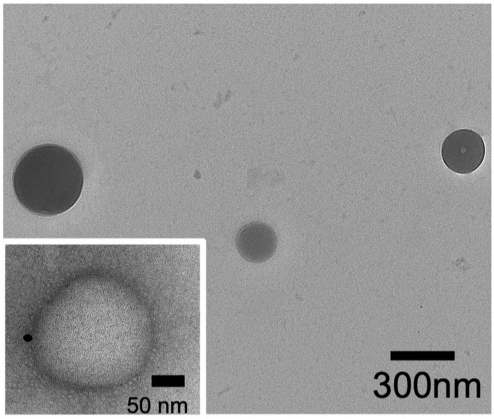

D

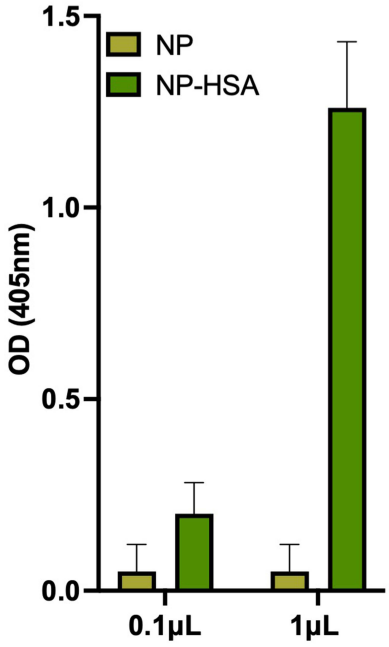

E

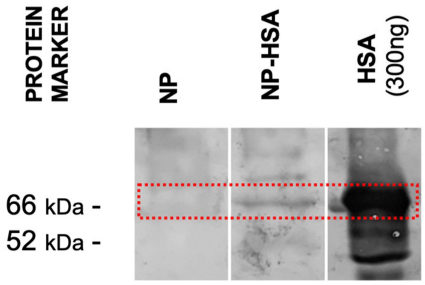

F

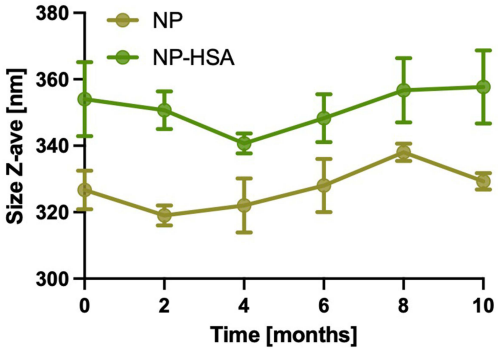

Figure 1 Characterization of nanoparticles (NPs) used for in vitro studies. (**A**) Summary table comparing the properties of uncoated nanoparticles (NP) and HSA-coated nanoparticles (NP-HSA), including encapsulated agent, average diameter, polydispersity index (PDI), and zeta potential. The NP-HSA formulation exhibits a slightly larger diameter and a less negative zeta potential compared to NP. Transmission electron microscopy (TEM) images showing the morphology of NP (**B**, scale bar 200nm) and NP-HSA (**C**, scale bar 300nm). Insets provide higher magnification views, indicating uniform spherical shapes of both nanoparticle formulations (scale bar 50 nm). (**D**) Sandwich ELISA to detect HSA presence on NP surface tested at different concentrations, as measured by optical density (OD). Data have been reported as the mean ± SD. (**E**) Western Blot analysis developed in non-reducing conditions to compare uncoated-NPs (NP) and NP-HSA to the positive control (HSA). (**F**) Long-term stability of NP and NP-HSA in PBS, showing the evolution of size (z-average) over 10 months, analyzed by DLS.

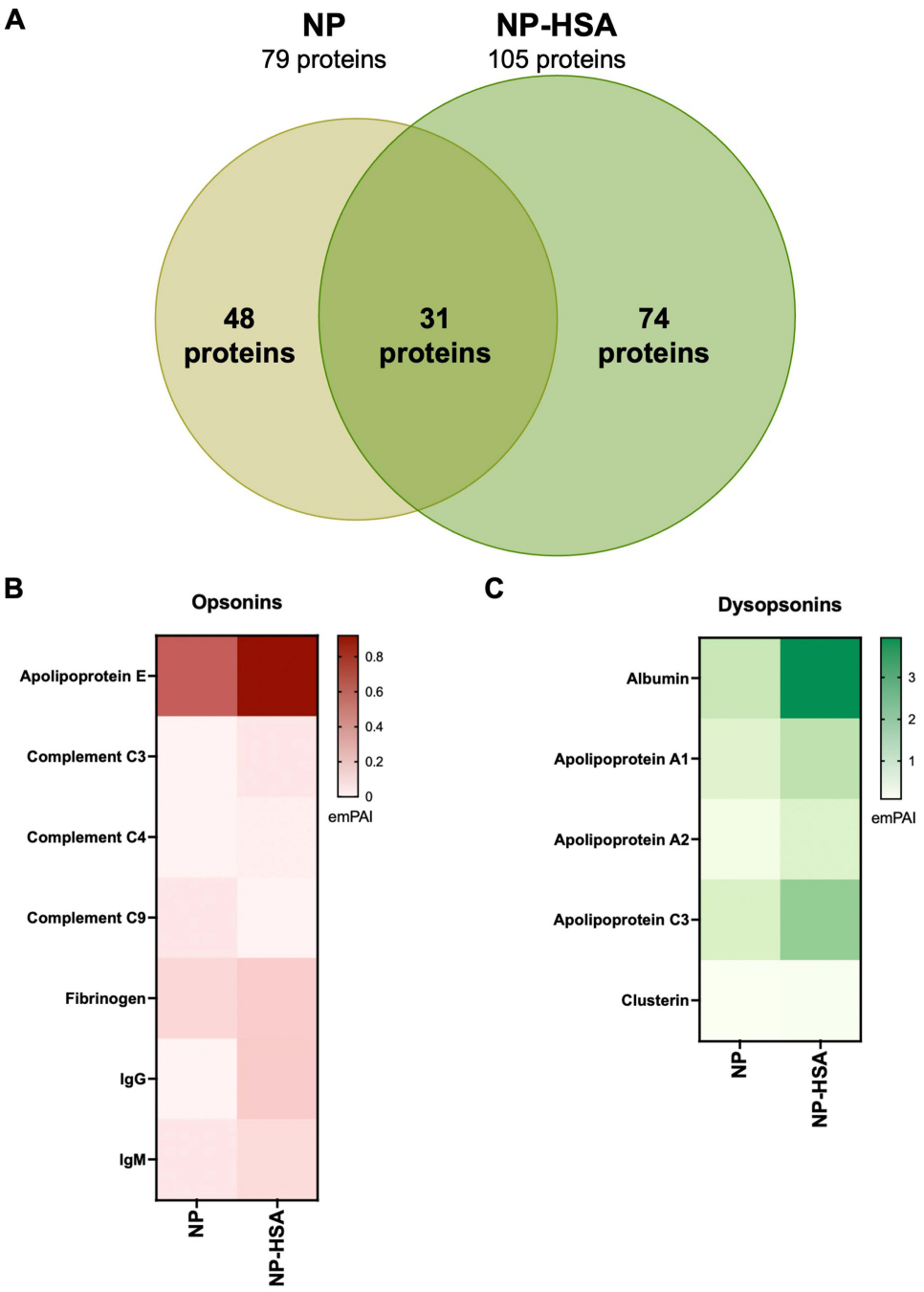

Figure 2 Data analysis from mass spectrometry. (**A**) NPs were incubated with Normal Human Serum (NHS) for 1h and analyzed by mass spectrometry. Venn diagram displaying the number of proteins adsorbed onto NP-HSA and NP. NP-HSA shows 79 unique proteins while NP has 105. Shared proteins between the two formulations are also highlighted. Differences in (**B**) opsonins and (**C**) dysopsonins adsorption between NP and NP-HSA. emPAI: exponentially modified Protein Abundance Index.

presence of C3 and C4, proteins of the early phase of the complement cascade, but no proteins of the terminal pathway were documented, evidence of an incomplete activation limited by dysopsonins.

The most represented opsonin on the surface of both NPs is the apolipoprotein E (apoE), which possesses a high affinity for the target, often forming part of the hard corona of NPs. Human albumin resulted as the prominent protein in the protein corona of both NPs, but the two preparations differed in the relative amount of HSA bound on their surface (Figure 2C). The proteomic data confirm that NP-HSA has a higher amount of this protein, probably deriving from both covalently bound and serum-derived albumin. In addition, other dysopsonins are more represented on NP-HSA if

compared to NP, including some apolipoproteins and clusterin (Figure 2C), suggesting that HSA coating can effectively increase NPs stealthiness preventing the phagocytosis of nanocarriers.

In vitro Nanoparticles Functional Characterization

NP and NP-HSA were in initially tested to evaluate direct lysis of red blood cells: no mechanical disruption of red blood cells by co-incubation with the NPs was documented (Figure 3A).

NP and NP-HSA were then incubated in human plasma and a Ca^{2+}-containing solution that induces the coagulation process and the clotting time was analyzed; NPs and control samples showed a very similar trend. The time required for the 50% coagulation was interpolated, showing no significant differences between the two preparations (Figure 3B) and indicating that these particles preserve biocompatibility with respect to the coagulation process.

Consumption of the complement system was also studied. LC-MS/MS showed the presence of IgG and IgM as well as of C3 and C4, prompting us to analyze the residual activity of the classical pathway after incubation of NHS with nanostructures. Decreased lytic activity in the NHS was observed because of the incubation with both preparations (Figure 3C).

The presence of covalent-bound HSA does not increase, but also does not decrease the capacity of these PLGA/PVA NPs to reduce complement activity.

The interaction between NPs and primary cells of the immune system was finally studied in vitro. White blood cells were recovered, and monocytes were separated from other leukocytes and activated as macrophages. Both populations were then incubated with the NPs pre-incubated with NHS and analyzed by flow cytometry. Data showed that HSA coating does not affect, as expected, the interaction and internalization with primary cells, such as leukocytes (Figure 3E). Most importantly, covalent-bound-HSA significantly prevented NP internalization by macrophages (Figure 3D), due to limited opsonization after NHS preincubation.

These data demonstrate that a permanent albumin coating changed the protein corona in favor of dysopsonins, markedly reducing phagocytosis by macrophages. It remains to be clarified if these new delivery platforms results to be effective also as a targeted drug delivery system for cancer treatment.

The Production and Characterization of the Targeting Mechanism

One of the main problems in cancer treatment is the need to increase the selectivity of drug treatments for the tumor target. Therefore, surface functionalization of drug delivery systems with agents that can specifically target tumors has become a globally accepted strategy. We choose CD19 proteins as the specific cell surface target and use an anti-CD19 antibody as the targeting agent. We selected the antibody MOR208, also known as tafasitamab, which was approved in 2020 for relapsed/refractory diffuse large B-cell lymphoma (DLBCL). The variable regions VH and VL of the original antibody were combined to form a scFv construct, which was finally fused to a human Fc fragment of an IgG1 (scFv-Fc, Figure 4A). The coding DNA sequence was optimized for secretion in CHO cells and then cloned into an eukaryotic expression vector. The recombinant antibody was affinity purified from the conditioned medium and analyzed by SDS-PAGE for purity and quantification. The correct molecular weight was also visualized by Western blot by comparing the unpurified supernatant to the different fractions and to a positive control (another scFv-Fc anti-CD20 produced in-house) (Figure 4A).

The capacity of the purified molecule to bind to CD19 antigen was analyzed by flow cytometry (Figures 4B and C) and fluorescence microscopy (Figures 4D and E). $CD19^+$ NALM-6 cells were incubated with anti-CD19 scFv-Fc or negative control, and the binding was visualized by a fluorescent-conjugated anti-human antibody, or incubated with PE-conjugated mouse antiCD19 IgG or isotypic controls. The fluorescent signal (green, Figure 4B, and red, Figure 4C) clearly increases in both samples incubated with anti-CD19 scFv-Fc (B, 97.2% positivity) or the positive control (C, 99.7% positivity) compared to cells incubated with the negative controls.

NALM-6 cells were also analyzed by fluorescence microscopy (Figure 4D, and E). NALM-6 cells (whose nuclei were stained with DAPI) were stained with negative control (Figure 4D, and E, lower right panels), or anti-CD19 scFv-Fc and a secondary antibody labeled with Alexa Fluor-488 (Figure 4D, green signal) or with the positive control PE (Figure 4E, red signal). These data confirmed that the purified scFv-Fc is able to bind $CD19^+$ cells as documented by flow cytometry.

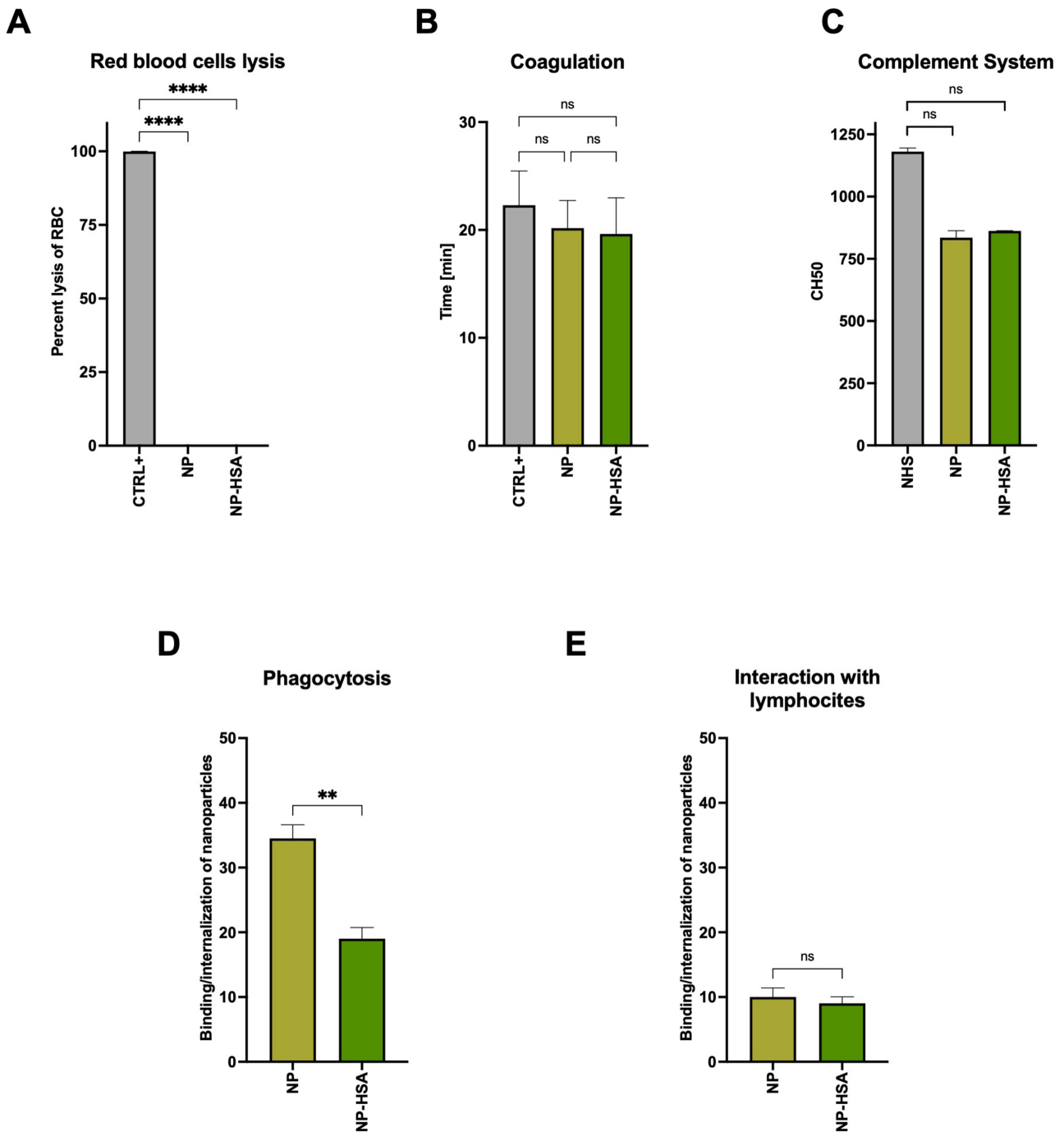

Figure 3 In vitro test for NPs functionality. (**A**) In vitro analysis of the direct lysis of the red blood cells. The in vitro turbidity curve trend of NP and NP-HSA in activated plasma during time was employed to extrapolate the (**B**) fifty percent coagulation time and data are shown as potential NPs effect on the coagulation system. (**C**) CH50 hemolytic activity was evaluated in NHS, as a control, and in the same NHS after 2 hours in vitro incubation with NP or NP-HSA. White cells were isolated from a healthy donor; 100,000 cells (monocytes or lymphocytes) were incubated in the presence of NHS with 4μL of uncoated (NP) and coated NPs (NP-HSA) at 37°C for 1 hour and analyzed by flow cytometry to evaluate the percentage of (**D**) phagocytosis or (**E**) the interaction of nanosystems with lymphocytes. Data are reported as the mean ± SD. Statistical analysis: t-tests. P ≤ 0.01 = **; P ≤ 0.0001 = ****, P≥0.05=ns.

In vitro Characterization of Targeted Nanodevice

The recombinant anti-CD19 scFv-Fc was employed to produce targeted NPs. An EDC/sulphoNHS linker was employed, and a mix of the recombinant scFv-Fc anti-CD19 and HSA were covalently bound to the surface of NPs, producing t-NP-HSA. The presence of both the HSA coating and the targeting agent was first confirmed by Western blot (Supplementary Figure 1A).

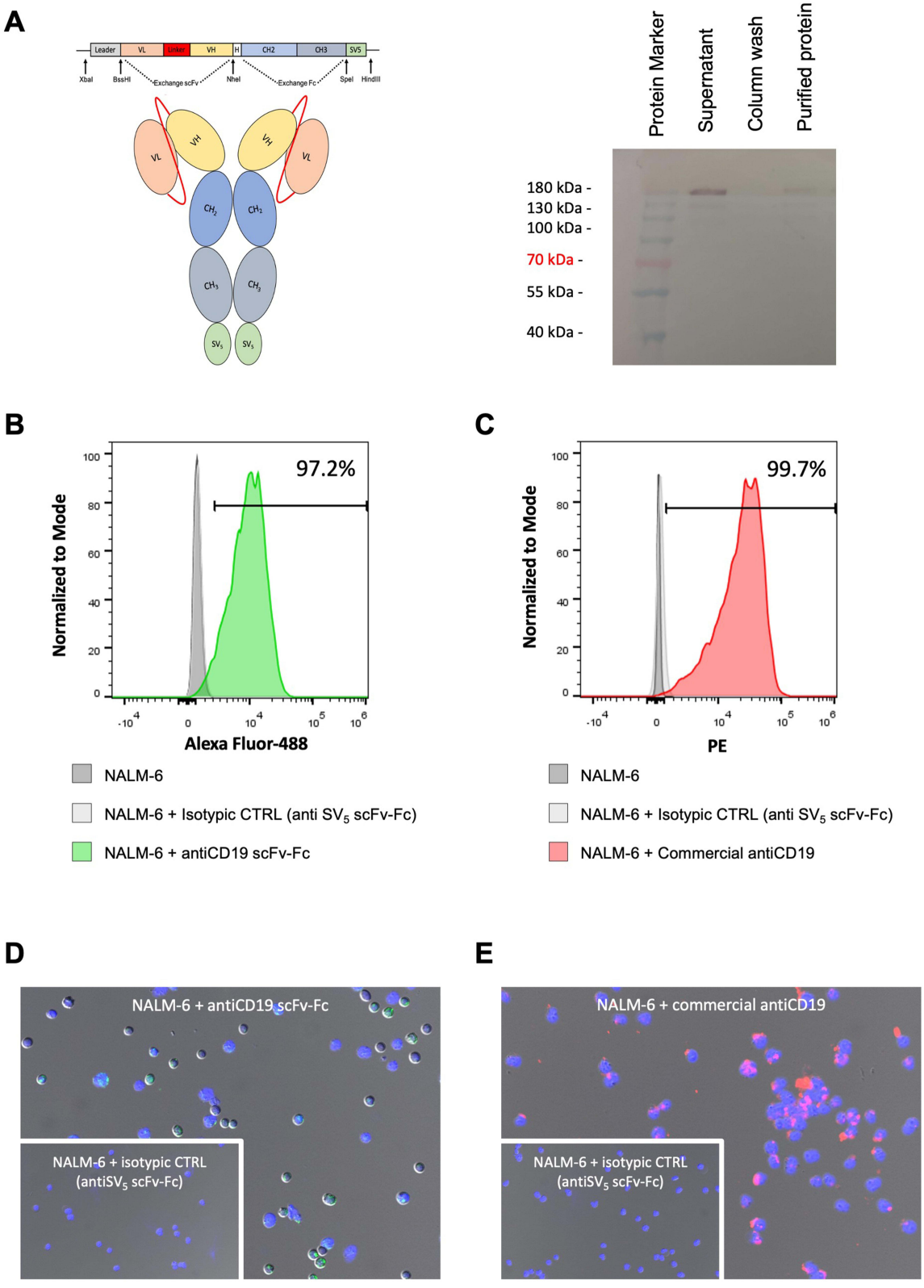

Figure 4 Design, production, and characterization of the targeting mechanism. (**A**) Schematic representation of the scFv-Fc construct. The published sequence of VH and VL regions of tafasitamab (MOR208), were obtained from its patent, optimized for CHO cells production, and then cloned in frame with Hinge-CH2-CH3-SV5 (tag) of human IgG1 in an expression vector. CHO-S cells were then transfected and screened to obtain a population of cells highly producing the anti-CD19 scFv-Fc (left). On the right, Western Blot analysis of protein purification shows the purified scFv-Fc anti-CD19 compared to the unpurified material. (**B-C**) Flow cytometry analysis of NALM-6 cells (250,000 cells) stained with 5ng/μL of anti-CD19 scFv-Fc (**B**, green, 97.2%) and 5ng/μL of commercial anti-CD19 (**C**, red, 99.7%) for 1h demonstrating high binding specificity compared to 5ng/μL of isotype controls (**B** and **C**, light grey). (**D-E**) Immunofluorescence microscopy images of NALM-6 cells (blue nuclei, DAPI) treated with anti-CD19 scFv-Fc (**D**, green) and commercial anti-CD19 (**E**, red). Insets show cells treated with isotype controls displaying no binding.

The NPs were then characterized for their physicochemical properties, comparing t-NP-HSA and non-targeted NP-HSA. The data confirm that the average diameter, PDI, and zeta potential values of the NPs are in the same range; anti-CD19 coupling increases the size from 348.7 ± 4.43 nm to 388.9 ± 1.99 nm and slightly increases the charge, which moves from 14.6 to −13.9mV. The regular round shape of the t-NP-HSA was verified and compared to NP-HSA by electron microscopy analysis (Supplementary Figures 1B for NP-HSA, and C for t-NP-HSA). Finally, the presence of both HSA coating (Supplementary Figure 1D) and the targeting agent (Supplementary Figure 1E) were also confirmed by ELISA assay. t-NP-HSA also showed good stability, as already described in general for the platform (Supplementary Figure 1F).

The protein corona composition of t-NP-HSA was investigated, by mass spectrometry, and compared with NP-HSA; data showed differences in the protein corona both in the number (Figure 5A) and in the composition (Supplementary Table 2) between the two samples. The presence of scFv-Fc was detected in t-NP-HSA as part of the IgG in the opsonins (Figure 5B) and the presence of albumin was confirmed in the dysopsonin (Figure 5C). In addition, among opsonins, and dysopsonins the comparison of their relative amount (Figure 5B) shows that both samples interact with opsonins on their surface. Fibrinogen was reduced in t-NP-HSA, apoE remains the most present on the surface of all NPs. The presence of IgG and IgM also on t-NP-HSA showed also deposition of complement proteins (C1q, C1s, C3, and C4); as for NP-HSA, they are restricted to the first part of the classical pathway. The absence of C5, C6, C7, C8, and C9 is evidence of an incomplete activation because of the presence of dysopsonins, like clusterin and vimentin, documented on t-NP-HSA (Figure 5C).

The compatibility of these NPs was then functionally characterized in vitro. t-NP-HSA and NP-HSA showed that they are not able to directly lyse red blood cells (Supplementary Figure 2A), while the targeting agent induces a slight acceleration of the coagulation (Supplementary Figure 2B) but does not enhance the activation of the classical pathway of the complement system (Supplementary Figure 2C). Anti-CD19 coupling does not modify the interaction and internalization with primary cells (Supplementary Figure 2E); in the leukocytes, the percentage of $CD19^+$ B-lymphocytes is minimal and does not allow to show the effect of the targeting agent. Most importantly, the targeting agent does not significantly increase the phagocytosis by macrophages (Supplementary Figure 2D).

The capacity of the targeting mechanism to cause binding/internalization in malignant B cells was tested by confocal microscopy. Cells were incubated with NP-HSA and t-NP-HSA in the presence of NHS, while cell membranes were visualized by Fast DiI and nuclei by DAPI. Confocal images showed that the NP-HSA were present almost only on the membrane (Figure 6A), whereas t-NP-HSA were visualized both on the membrane and inside the cells (Figure 6B). These data confirm the ability of anti-CD19 to increase the nanostructure's internalization rate, as previously shown for other polymeric NPs. Indeed, there was a significant difference between the 80% of t-NP-HSA internalized, compared to about 20% that was still on the cell surface. In contrast, the internalization rate of nontargeted nanoparticles (NP-HSA) was about 70%, whereas 30% were located on the membrane (Figure 6C).

The phagocytosis of NP-HSA and t-NP-HSA was deeply studied using differentiated THP-1 cells, as performed before; cells were differentiated and incubated for 1h with NP-HSA and t-NP-HSA in the presence of NHS, and confocal microscopy was used to visualize the samples (Figures 6D, and E). Both NPs were mainly localized on the external side of the cellular membrane, demonstrating that the presence of the targeting mechanism does not affect the ability of covalently bound HSA (present in both the targeted and nontargeted nanostructures) to prevent nanoparticle phagocytosis (Figure 6F).

Targeted Nano-Devices: In vivo Characterization

Embryos from the transgenic Tg (mpeg1:mCherry) zebrafish strain were used to study NPs behavior in vivo. A tumor-bearing zebrafish model was initially established by injecting labeled NALM-6 cells into the duct of Cuvier at 48 hours post fertilization (hpf) and followed over time. NALM-6 cells were widely distributed in the zebrafish body, with a preferential accumulation in the posterior blood island, described also as a macrophage-rich area (Figure 7A). The Corrected Total Cell Fluorescence (CTCF) of the distributed cells was quantified 24 hours after injection in three different groups, demonstrating the reproducibility of the model (Figure 7B). Survival was also analyzed by comparing Kaplan-Mayer obtained from control zebrafish and NALM-6-bearing zebrafish; results show that 80% of zebrafish

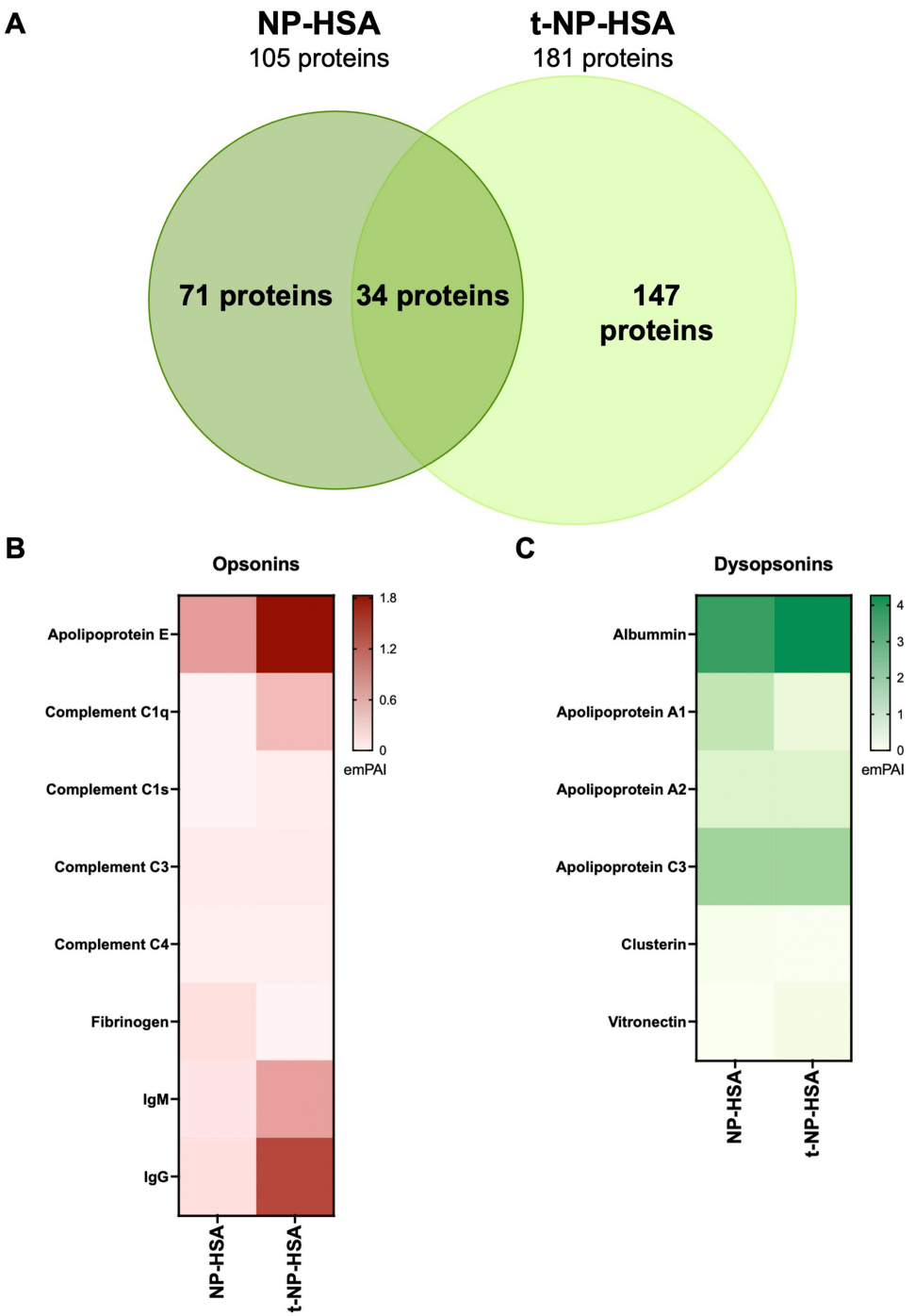

Figure 5 Data analysis from mass spectrometry. (**A**) NPs were incubated with NHS for 1h and analyzed by mass spectrometry. Venn diagram displaying the number of proteins adsorbed onto NP-HSA and t-NP-HSA. The analysis highlighted 105 proteins for the NP-HSA sample and 181 for t-NP-HSA. 71 proteins were specific for NP-HSA, 147 proteins were specific for t-NP-HSA, and 34 proteins were present on both NPs. Differences in (**B**) opsonins and (**C**) dysopsonins adsorption between NP-HSA and t-NP-HSA. emPAI: exponentially modified Protein Abundance Index.

receiving human cells did not survive beyond 2 dpi. At the end of the study, only 3 larvae out of 30 receiving NALM-6 survived, while 96.6% of the control animals survived (Figure 7C).

This model was initially used to analyze the NP distribution; zebrafish embryos received NALM-6 cells and fluorescent NPs were injected 4 hours later. Animals were visualized by fluorescence microscopy immediately after NP injection and after 24h and the biodistribution data were expressed as the percentage of NPs localized in the different

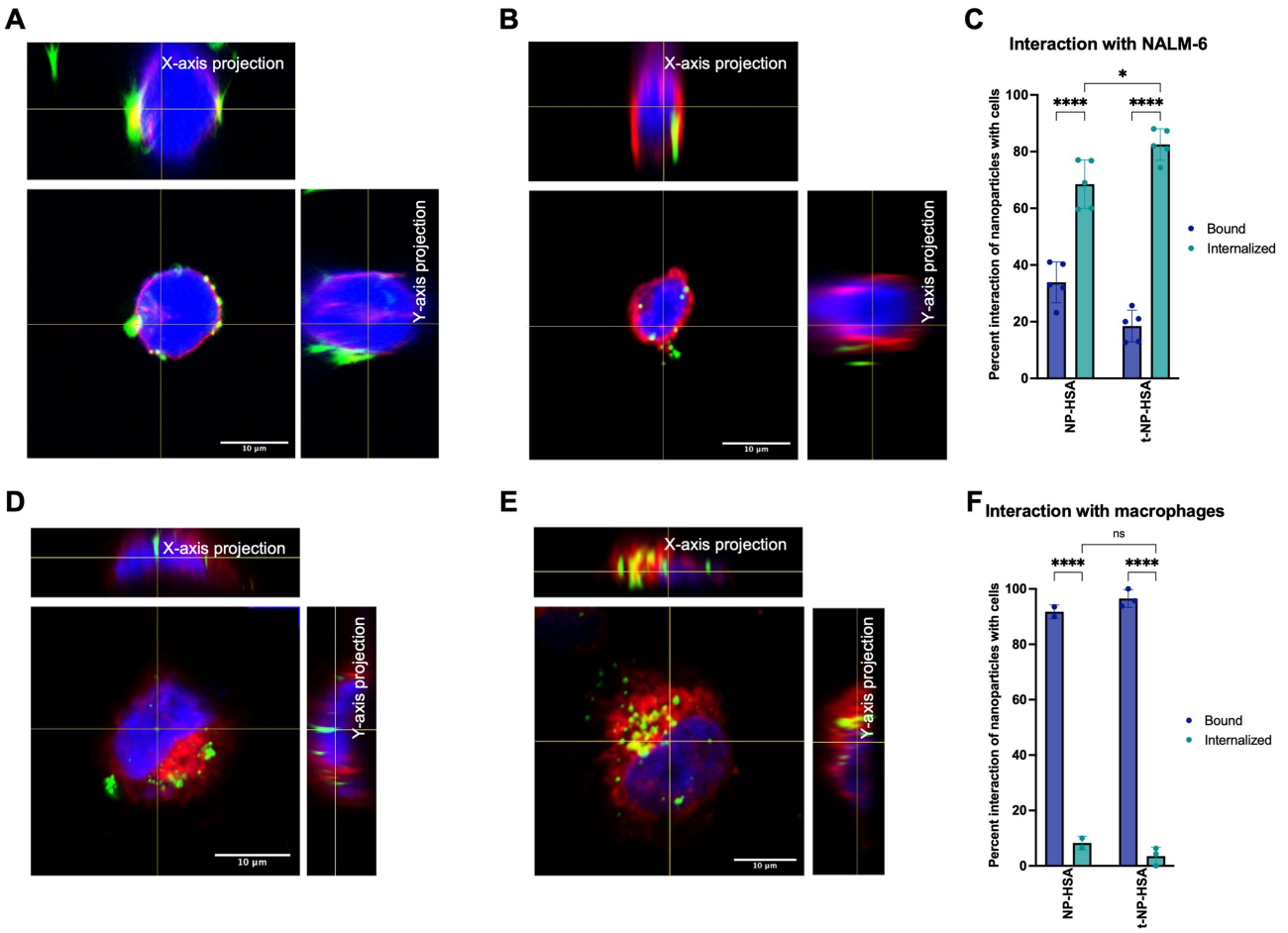

Figure 6 Localization of NP inside cells. 250,000 NALM-6 cells were incubated with 2µL of NPs in the presence of NHS, membranes were labeled with Vybrant Fast DiI, and the nuclei with DAPI. (**A**) Green-fluorescent NP-HSA (untargeted-NPs) are localized almost exclusively on the red-fluorescent membrane, while (**B**) green-fluorescent t-NP-HSA (targeted-NPs) are localized both on the red-fluorescent membrane and in the blue-fluorescent-nuclei. X- and Y-axis projections highlight the internalization process. (**C**) Targeted (t-NP-HSA) and untargeted particles (NP-HSA) were counted with Fiji software and represented as a percentage of bound and internalized. Data confirmed that targeted-NPs are statistically more internalized than bound to the membranes are more than targeted-NPs and parallely more targeted-NPs are internalized than untargeted-ones. 100,000 THP-1 cells were differentiated in macrophages (100ng/mL of PMA) incubated with 2µL of NPs in the presence of NHS, membranes were labeled with VybrantTM Fast DiI, and the nuclei with DAPI. (**D**) green-fluorescent NP-HSA (untargeted-NPs) and (**E**) green-fluorescent t-NP-HSA (targeted-NPs) are both localized more on the red-fluorescent membrane than in the blue-fluorescent nuclei. X- and Y-axis projections highlight the internalization process. (**F**) Targeted (t-NP-HSA) and untargeted particles (NP-HSA) were counted with Fiji software and represented as a percentage of bound and internalized. Data confirmed that both preparations are statistically more bound than internalized to the membranes, confirming the importance of the HSA (present in both preparations) to prevent their phagocytosis. Data are reported as the mean ± SD. Statistical analysis: two-way ANOVA. $P \leq 0.05$ = *; $P \leq 0.0001$ = ****.

tissues. More than 60% of both nontargeted (NP-HSA) and targeted NPs (t-NP-HSA) remained in the bloodstream (Figure 7D) and are still available for interaction with the target. On the other hand, less than 25% of the injected NPs were phagocytosed by macrophages (Figure 7E), without significant differences caused by the presence of the targeting agent. For what concerns the in vivo interaction with target cells, t-NP-HSA shows a colocalization rate three times higher than untargeted-NPs (~15% versus ~5%, Figure 7F). Since, also in vivo, the HSA coating reduces the phagocytosis and the recombinant antibody enhances the interaction with $CD19^+$ cancer cells, the t-NP-HSA was chosen as the optimal delivering system for the treatment of B-cell malignancies.

In vivo Efficacy of Drug-Loaded Nanoparticles for B-Cell Malignancies Treatment

Doxorubicin was selected as a candidate for encapsulation in HSA-covered targeted PLGA-PVA structures. Doxorubicin-loaded NPs were prepared with a covalently bound albumin coating and an anti-CD19 targeting mechanism (doxo-t-NP). The NPs exhibited sizes less than 500 nm, a moderate negative surface charge (−0.22 ± 0.06), and the encapsulation efficiency was evaluated as previously performed.

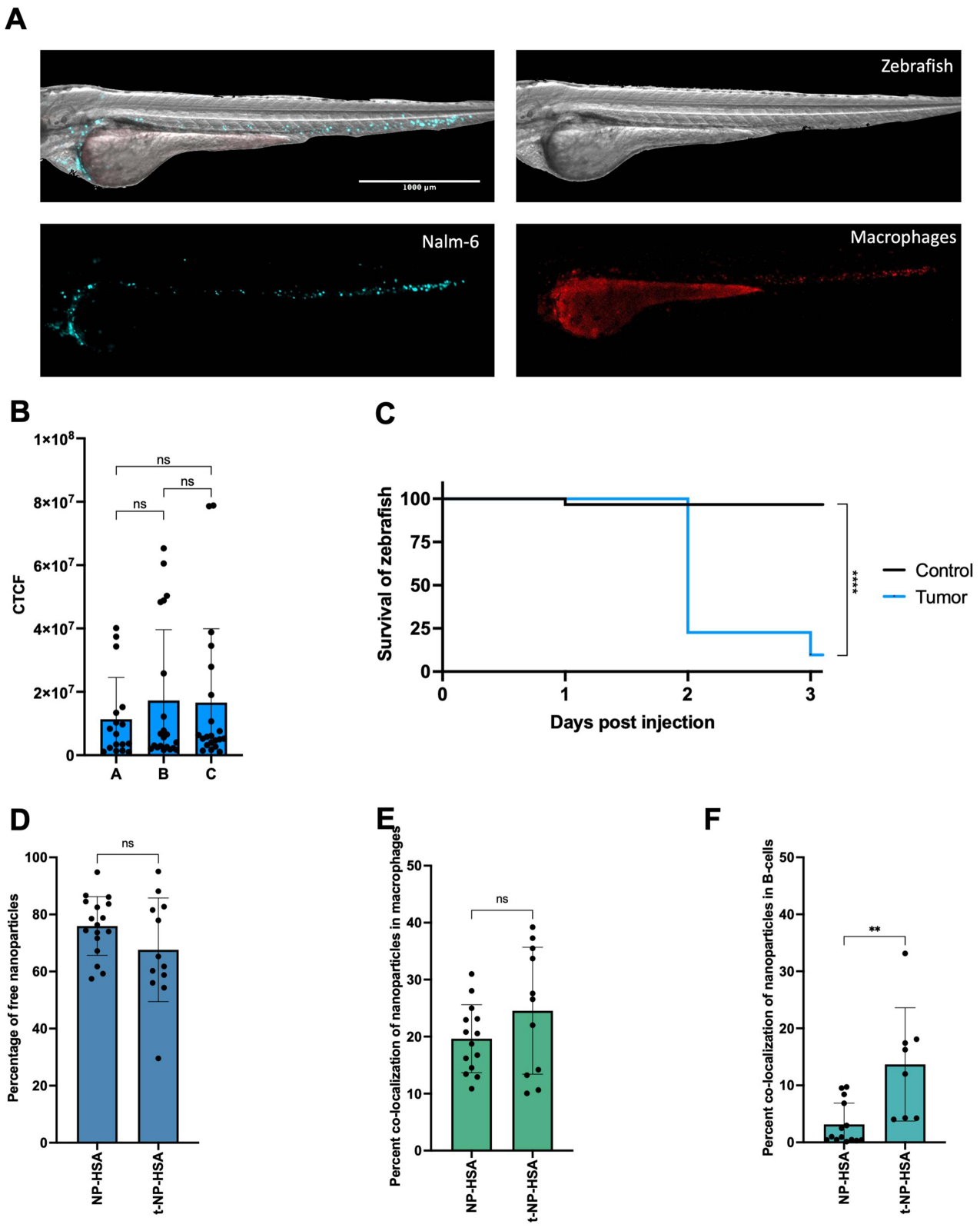

Figure 7 Setting up of the animal model and biodistribution studies. (**A**) 500 NALM-6 cells, labeled with VybrantTM Fast DiD (near-infrared fluorescent dye, lower left panel) were injected 2dpf in the duct of Cuvier of Tg (mpeg1:mCherry) transgenic zebrafish (upper right panel), which possess red-fluorescent macrophages (lower right panel). (**B**) Data analysis of the CTCF of the near-infrared-fluorescent areas (NALM-6 cells) of zebrafish randomly assigned to three different groups, suggesting that the three groups received the same number of cells. (**C**) Zebrafish (nControl=30, nTumor=30) received NALM-6 cells (500) and animal survival was represented as Kaplan Mayer curve. Statistical analysis: Log rank test. Control vs tumor: P-value ≤ 0.0001 = ****. Fluorescent NPs were injected in this zebrafish model and the biodistribution was evaluated. (**D**) Comparison of the percentage between NP-HSA and t-NP-HSA, not yet internalized by cells or macrophages. (**E**) The percentage of the macrophages' internalization of NP-HSA or t-NP-HSA. (**F**) The percentage of the internalization of NP-HSA or t-NP-HSA in tumor B-cells. All data report as the mean ± SD. Statistical analysis: *t*-test. P ≤ 0.05 = **, P≥0.05=ns.

To evaluate the therapeutic efficacy of doxo-t-NP, the human-zebrafish model of diffuse ALL was induced in the transgenic Tg (fli1:EGFP) line, showing green fluorescent blood vessels, in order to better appreciate the spreading of cells in the zebrafish body.

Calcein-AM-labeled NALM-6 cells were injected into the duct of Cuvier of zebrafish embryos, and after 4 hours, free doxorubicin (4,6nL of 1µM final concentration) or doxo-t-NP (targeted doxorubicin-loaded NPs, 4,6nL of 1µM of encapsulated doxorubicin) was injected. Zebrafish survival was monitored up to 3dpi (Figure 8A) demonstrating that doxo-t-NP were as effective as the free drug, resulting in an increase in animal survival of approximately 30% compared to saline-treated zebrafish.

Zebrafish were also examined by fluorescence microscopy immediately after (Figure 8B, upper panels, 0hpi) and 24 hours after NP injection (Figure 8B, lower panels, 24 hours). NALM-6 cells were initially distributed throughout the body, but their fluorescence signal was almost abolished 24 hours later by treatment with doxo-t-NP. CTCF was calculated as previously described at 0hpi and compared with data at 24hpi in 3 groups of NALM-6-bearing embryos

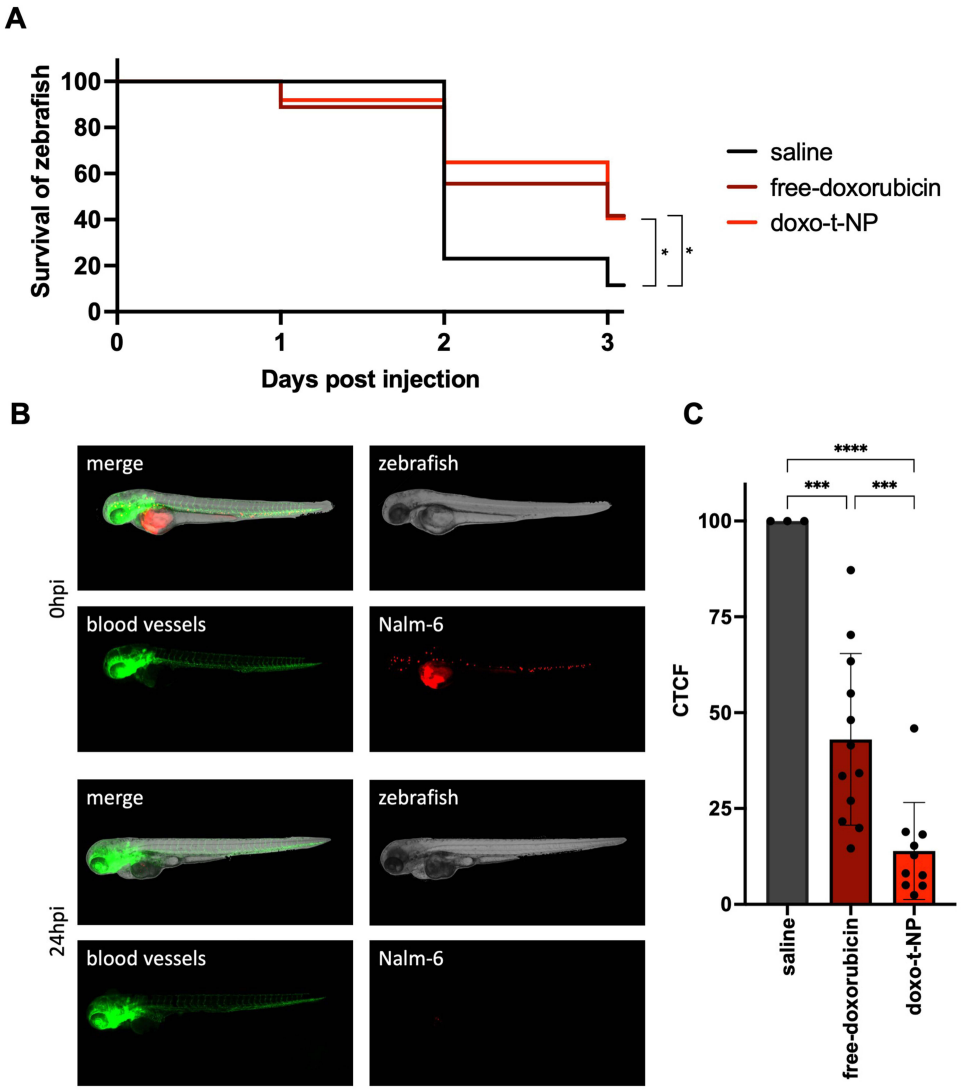

Figure 8 Therapeutic effect of doxo-t-NP in a diffused model of B-cell malignancy. (**A**) Zebrafish (nSaline=26, nFree-doxorubicin=37, ndoxo-t-NP=36) received NALM-6 cells (500, labeled with red-fluorescent Calcein-AM) and 4h later, 4,6nL of saline or free-doxorubicin or doxo-t-NP (targeted-, doxorubicin-loaded-NPs). Animal survival was represented as the Kaplan Mayer curve. Statistical analysis: Log rank test. P-value ≤ 0.01 = *. (**B**) Zebrafish were analyzed immediately after the injection of NPs (upper panels) and 24hpi (lower panels) through fluorescence microscopy. (**C**) Data analysis of the CTCF after treatment with free-doxorubicin or doxo-t-NP expressed as a percentage. All data is reported as the mean ± SD. Statistical analysis: one-way ANOVA. P ≤ 0.001 = ***; P ≤ 0.0001 = ****. The table of contents entry should be 50–60 words long and should be written in the present tense. The text should be different from the abstract text.

treated with saline, free doxorubicin, or doxo-t-NPs, respectively (Figure 8C); variation of the fluorescence signal in each animal showed that free doxorubicin was able to significantly reduce tumor cell burden compared with saline-treated zebrafish. This result was even more pronounced in doxo-t-NP treated animals, suggesting that this delivery platform should reduce doxorubicin side effects, increasing specificity and, as a consequence, the drug efficacy.

Discussion

Nanocarriers represent a great innovation in the delivery of drugs and probes in specific microenvironments or to specific cells, aiming to guarantee a localized activity and minimize the side effects. Unfortunately, their clinical application is deeply limited by the fast elimination; in particular, nanostructures are often recognized as not "self" and opsonized by immunoglobulins, complement components, and coagulation proteins, in the context of the protein corona formed on NPs in the bloodstream. Opsonins can be recognized by specific receptors expressed on the surface of resident phagocytic cells present mainly in the liver, but also the spleen and lungs, and this is the major cause of nanoparticle elimination from the blood.[7,8] The analysis of the protein corona deposited on different particles evidenced a dynamic evolvement of its composition, which begins with proteins forming a 'soft corona' that are rapidly substituted by other proteins developing a 'hard corona', that include opsonins. This analysis also showed that other serum proteins are part of the protein corona, including dysopsonins, which can prevent the absorption of opsonins and finally reduce their clearance.[37] Examples of dysopsonins are apolipoproteins and regulators of the complement system, but the most abundant dysopsonin is albumin;[9] this protein is initially present also in the soft corona and its binding is due to the high concentration in the plasma; in the formation of the hard corona, it is easily displaced by opsonins because the interaction with NPs is typically allowed by weak bonds, like hydrogen bonds and van der Waals interactions.[37]

Our results demonstrated that it is possible to prepare polymeric NPs[35,38] with a covalent binding of HSA, in order to mimic soft corona and to prevent the binding of opsonins. The covalent coating of NPs with the most abundant dysopsonin in the bloodstream can hide polymeric nanodevices from elimination by the immune system.[37]

HSA-decorated NPs did not change the physicochemical properties of the structures, which confirms data obtained with similar polymeric particles or studying the binding of different proteins, like antibodies, antibody fragments, or enzymes.[38,39] The composition of the protein corona was characterized, showing that the presence of the coating affects the relative abundance of opsonins, in favor of dysopsonins.[40] In general, the presence of a higher number of proteins, specific for NP-HSA, can be explained by the capacity of albumin to interact with several serum proteins, as in the formation of soft corona, but not eliminated during the detachment of albumin in the formation of hard corona.[12] The most represented opsonin on the surface of both NPs is apoE, usually part of the hard corona of NPs. It contains an LDL-receptor binding domain and this aspect can facilitate the target of cancer cells that overexpress LDL receptors.[41] The increased amount of apoE on NP-HSA can also derive from its ability to bind HSA;[42] also the fibrinogen amount resulted in be increase but also this protein is able to bind to albumin fragments.[43] Functional tests will be important to clarify if albumin-bound proteins are activated, act as opsonins, and increase elimination by macrophages, or if they are only bound molecules, not influencing opsonization, not recognized by their receptors, and not enhancing NPs phagocytosis. At the same time, other dysopsonins were more present on NP-HSA if compared to NP, including some apolipoproteins and clusterin, suggesting that HSA coating can effectively increase NPs stealthiness preventing the phagocytosis of nanocarriers. These results are also consistent with previous studies on other NP types,[44] suggesting that the final balance between opsonins and dysopsonins can predict the in vivo activity and clearance.[45]

These polymeric NPs, independently from the presence of HSA, did not interfere with red blood cells or the coagulation process but a decreased lytic activity of the NHS was observed after incubation with both preparations. This could be due to a partial consumption of complement proteins by adsorption on the surface of NPs, although mass spectrometry data do not allow discrimination between inactive (eg C3) and activated proteins (eg C3b) bound to the surface of NP, as we have previously demonstrated for similar polymeric NP.[37]

HSA-covered PLA-PVA NPs finally represent a safe nanoplatform, less internalized by phagocytic cells than uncoated NPs.

A second important factor that influences the activity of a nanoplatform is its capacity to select a specific cellular target; surface functionalization of delivery systems with agents that can specifically target tumor cells is an example of

this standardized approach.[46,47] The stealthy effect caused by covalent-bound-HSA remains evident also in the presence of surface antibodies as a targeting agent.

An anti-CD19 recombinant antibody has been chosen as a prototype of a molecule able to specifically target $CD19^+$ B-cells.[48,49] Targeted-HSA-NPs maintained the opsonin/dysopsonin ratio that prevents phagocytosis by macrophages but guarantees a preferential internalization in $CD19^+$ ALL tumor cells.[46,47,50]

In the management of ALL, anthracyclines are a prominent class of chemotherapeutic agents known for their mechanism of action, which involves DNA intercalation and disruption of DNA metabolism and RNA synthesis. The primary dose-limiting toxicities associated with free anthracyclines are myelosuppression and cardiotoxicity;[51] our group has successfully demonstrated that doxorubicin-loaded PLGA-PVA NPs are safe and can arrest tumor growth in a localized model of B-cell malignancies.[34] In a localized disease model, it is relatively straightforward to exploit the EPR effect with larger NPs. However, in the context of a disseminated pathology, the targeting mechanism becomes crucial to specifically reach and affect cancer cells. Indeed, anti-CD19 t-HSA-NP loaded with doxorubicin reduces tumor burden and increases animal survival in a human-zebrafish model of ALL.[34,52] This represents a promising approach for treating B-cell malignancies. More in general, PLGA-PVA NPs are biodegradable and safe; the albumin, stably on the surface, hides the nanodevices from the immune system, which increases the circulation time of the NPs, and the targeting recombinant antibody guarantees that the target is reached, reducing potential off-target effects.

These nanostructures represent a nanoplatform, where the individual parts (payload or the targeting mechanism) can be tailored for the diagnosis or treatment of various diseases.

Conclusion

The covalent coating of NPs with the most abundant dysopsonin in the bloodstream can hide polymeric nanodevices from elimination by the immune system. The composition of the protein corona was characterized, showing that the presence of the coating affects the relative abundance of opsonins and dysopsonins. This nanoplatform is found to be safe, and less internalized by phagocytic cells than uncoated NPs.

The stealthy effect also remains evident in the presence of a surface antibody as a targeting agent. CD19 t-HSA-NP loaded with doxorubicin reduces tumor burden and increases animal survival in a human-zebrafish model of ALL. This is a promising tool for the treatment of B-cell malignancies, but it is also the result of a platform that can be used for other pathologies. The PLGA-PVA NPs are biodegradable and safe. In addition, the albumin coating hides the nanodevices from the immune system, which increases the circulation time of the NPs, and the targeting mechanism ensures that the target is reached, reducing potential off-target effects.

These nanostructures can be considered as a nanoplatform, where the individual components, such as the payload or the targeting mechanism, can be tailored for the diagnosis or treatment of various diseases.

Acknowledgments

The authors thank Dr. Paolo Bertoncin for his support in EM analysis at the Dept of Life Sciences – University of Trieste, and Dr. Paolo Durigutto for his support during functional characterization.

Author Contributions

All authors made a significant contribution to the work reported, whether that is in the conception, study design, execution, acquisition of data, analysis and interpretation, or in all these areas; took part in drafting, revising or critically reviewing the article; gave final approval of the version to be published; have agreed on the journal to which the article has been submitted; and agree to be accountable for all aspect of the work.

Funding

The research leading to these results was supported by funds from the University of Trieste and AIRC (12965) to Paolo Macor, and from the European Union - NextGenerationEU through the Italian Ministry of University and Research under PNRR - M4C2-I1.3 Project PE_00000019 “HEAL ITALIA” to Giuseppe Toffoli (Spoke 6) (CUP J33C22002930006 of Centro di Riferimento Oncologico di Aviano, IRCCS). The views and opinions expressed are those of the authors only

and do not necessarily reflect those of the European Union or the European Commission. Neither the European Union nor the European Commission can be held responsible for them.

Disclosure

The authors report no conflicts of interest in this work.

References

1. Farokhzad OC, Langer R. Impact of nanotechnology on drug delivery. *ACS Nano*. 2009;3(1):16–20. doi:10.1021/nn900002m
2. Bozzer S, Dal Bo M, Grimaldi MC, Toffoli G, Macor P. Nanocarriers as a delivery platform for anticancer treatment: biological limits and perspectives in B-cell malignancies. *Pharmaceutics*. 2022;14(9):1965. doi:10.3390/pharmaceutics14091965
3. Yang F, Xue J, Wang G, Diao Q. Nanoparticle-based drug delivery systems for the treatment of cardiovascular diseases. *Front Pharmacol*. 2022;13:999404. doi:10.3389/fphar.2022.999404
4. Sinha R, Kim GJ, Nie S, Shin DM. Nanotechnology in cancer therapeutics: bioconjugated nanoparticles for drug delivery. *Mol Cancer Ther*. 2006;5 (8):1909–1917. doi:10.1158/1535-7163.MCT-06-0141
5. Danhier F. To exploit the tumor microenvironment: since the EPR effect fails in the clinic, what is the future of nanomedicine? *J Control Release*. 2016;244(Pt A):108–121. doi:10.1016/j.jconrel.2016.11.015
6. Albert C, Huang N, Tsapis N, et al. Bare and sterically stabilized PLGA nanoparticles for the stabilization of Pickering emulsions. *Langmuir*. 2018;34(46):13935–13945. doi:10.1021/acs.langmuir.8b02558
7. Lorenzer C, Dirin M, Winkler AM, Baumann V, Winkler J. Going beyond the liver: progress and challenges of targeted delivery of siRNA therapeutics. *J Control Release*. 2015;203:1–15. doi:10.1016/j.jconrel.2015.02.003
8. Baboci L, Capolla S, Di Cintio F, et al. The dual role of the liver in nanomedicine as an actor in the elimination of nanostructures or a therapeutic target. *J Oncol*. 2020;2020:4638192. doi:10.1155/2020/4638192
9. Panico S, Capolla S, Bozzer S, Toffoli G, Dal Bo M, Macor P. Biological features of nanoparticles: protein Corona formation and interaction with the immune system. *Pharmaceutics*. 2022;14(12):2605. doi:10.3390/pharmaceutics14122605
10. Jokerst JV, Lobovkina T, Zare RN, Gambhir SS. Nanoparticle PEGylation for imaging and therapy. *Nanomedicine*. 2011;6(4):715–728. doi:10.2217/nnm.11.19
11. Wang R, Zhang Z, Liu B, et al. Strategies for the design of nanoparticles: starting with long-circulating nanoparticles, from lab to clinic. *Biomater Sci*. 2021;9(10):3621–3637. doi:10.1039/d0bm02221g
12. Hyun H, Park J, Willis K, et al. Surface modification of polymer nanoparticles with native albumin for enhancing drug delivery to solid tumors. *Biomaterials*. 2018;180:206–224. doi:10.1016/j.biomaterials.2018.07.024
13. Li Y, Lee JS. Insights into characterization methods and biomedical applications of nanoparticle-protein Corona. *Materials*. 2020;13(14). doi:10.3390/ma13143093
14. Tao X, Zhang Q, Ling K, et al. Effect of pullulan nanoparticle surface charges on HSA complexation and drug release behavior of HSA-bound nanoparticles. *PLoS One*. 2012;7(11):e49304. doi:10.1371/journal.pone.0049304
15. Peng Q, Zhang S, Yang Q, et al. Preformed albumin Corona, a protective coating for nanoparticles based drug delivery system. *Biomaterials*. 2013;34(33):8521–8530. doi:10.1016/j.biomaterials.2013.07.102
16. Mocan L, Matea C, Tabaran FA, et al. Selective ex vivo photothermal nano-therapy of solid liver tumors mediated by albumin conjugated gold nanoparticles. *Biomaterials*. 2017;119:33–42. doi:10.1016/j.biomaterials.2016.12.009
17. Berrecoso G, Crecente-Campo J, Alonso MJ. Unveiling the pitfalls of the protein Corona of polymeric drug nanocarriers. *Drug Deliv Transl Res*. 2020;10(3):730–750. doi:10.1007/s13346-020-00745-0
18. Bertrand N, Wu J, Xu X, Kamaly N, Farokhzad OC. Cancer nanotechnology: the impact of passive and active targeting in the era of modern cancer biology. *Adv Drug Deliv Rev*. 2014;66:2–25. doi:10.1016/j.addr.2013.11.009
19. Sanna V, Pala N, Sechi M. Targeted therapy using nanotechnology: focus on cancer. *Int J Nanomed*. 2014;9:467–483. doi:10.2147/IJN.S36654
20. Dai W, Wang X, Song G, et al. Combination antitumor therapy with targeted dual-nanomedicines. *Adv Drug Deliv Rev*. 2017;115:23–45. doi:10.1016/j.addr.2017.03.001
21. Kamaly N, Yameen B, Wu J, Farokhzad OC. Degradable controlled-release polymers and polymeric nanoparticles: mechanisms of controlling drug release. *Chem Rev*. 2016;116(4):2602–2663. doi:10.1021/acs.chemrev.5b00346
22. Houshmand M, Garello F, Circosta P, et al. Nanocarriers as magic bullets in the treatment of leukemia. *Nanomaterials*. 2020;10(2):276. doi:10.3390/nano10020276
23. Tedder TF, Engel P. CD20: a regulator of cell-cycle progression of B lymphocytes. *Immunol Today*. 1994;15(9):450–454. doi:10.1016/0167-5699(94)90276-3
24. Krackhardt AM, Witzens M, Harig S, et al. Identification of tumor-associated antigens in chronic lymphocytic leukemia by SEREX. *Blood*. 2002;100(6):2123–2131. doi:10.1182/blood-2002-02-0513
25. Muggen AF, Pillai SY, Kil LP, et al. Basal Ca(2+) signaling is particularly increased in mutated chronic lymphocytic leukemia. *Leukemia*. 2015;29 (2):321–328. doi:10.1038/leu.2014.188
26. Jeong K, Kang CS, Kim Y, Lee YD, Kwon IC, Kim S. Development of highly efficient nanocarrier-mediated delivery approaches for cancer therapy. *Cancer Lett*. 2016;374(1):31–43. doi:10.1016/j.canlet.2016.01.050
27. Raufi A, Ebrahim AS, Al-Katib A. Targeting CD19 in B-cell lymphoma: emerging role of SAR3419. *Cancer Manag Res*. 2013;5:225–233. doi:10.2147/CMAR.S45957
28. Yi JH. Novel combination immunochemotherapy beyond CD20 for B-cell lymphomas. *Blood Res*. 2021;56(S1):S1–S4. doi:10.5045/br.2021.2020320
29. Capolla S, Argenziano M, Bozzer S, et al. Targeted chitosan nanobubbles as a strategy to down-regulate microRNA-17 into B-cell lymphoma models. *Front Immunol*. 2023;14:1200310. doi:10.3389/fimmu.2023.1200310

30. Li X, Ding Y, Zi M, et al. CD19, from bench to bedside. *Immunol Lett*. 2017;183:86–95. doi:10.1016/j.imlet.2017.01.010
31. Sadelain M, Brentjens R, Riviere I. The basic principles of chimeric antigen receptor design. *Cancer Discov*. 2013;3(4):388–398. doi:10.1158/2159-8290.CD-12-0548
32. Watkins MP, Bartlett NL. CD19-targeted immunotherapies for treatment of patients with non-Hodgkin B-cell lymphomas. *Expert Opin Investig Drugs*. 2018;27(7):601–611. doi:10.1080/13543784.2018.1492549
33. Bozzer S Preclinical development of targeted-nanoparticles for the treatment of pediatric B-cell malignancies acute lymphoblastic leukemia and Burkitt lymphoma. Università degli Studi di Trieste; 2022. Available from: https://hdl.handle.net/11368/3030999. Accessed December 04, 2024.
34. Bozzer S, De Maso L, Grimaldi MC, et al. Zebrafish: a useful animal model for the characterization of drug-loaded polymeric NPs. *Biomedicines*. 2022;10(9):2252. doi:10.3390/biomedicines10092252
35. Vasir JK, Labhasetwar V. Preparation of biodegradable nanoparticles and their use in transfection. *CSH Protoc*. 2008;2008:pdbprot4888. doi:10.1101/pdb.prot4888
36. Manfredi M, Martinotti S, Gosetti F, Ranzato E, Marengo E. The secretome signature of malignant mesothelioma cell lines. *J Proteomics*. 2016;145:3–10. doi:10.1016/j.jprot.2016.02.021
37. Capolla S, Colombo F, De Maso L, et al. Surface antibody changes protein Corona both in human and mouse serum but not final opsonization and elimination of targeted polymeric nanoparticles. *J Nanobiotechnol*. 2023;21(1):376. doi:10.1186/s12951-023-02134-4
38. Colombo F, Durigutto P, De Maso L, et al. Targeting CD34(+) cells of the inflamed synovial endothelium by guided nanoparticles for the treatment of rheumatoid arthritis. *J Autoimmun*. 2019;103:102288. doi:10.1016/j.jaut.2019.05.016
39. Macor P, Durigutto P, Argenziano M, et al. Plasminogen activator-coated nanobubbles targeting cellbound beta2-glycoprotein I as a novel thrombus-specific thrombolytic strategy. *Haematologica*. 2023;108(7):1861–1872. doi:10.3324/haematol.2022.281505
40. Papini E, Tavano R, Mancin F. Opsonins and dysopsonins of nanoparticles: facts, concepts, and methodological guidelines. *Front Immunol*. 2020;11:567365. doi:10.3389/fimmu.2020.567365
41. Yeo ELL, Cheah JUJ, Thong PSP, Soo KC, Kah JCY. Gold nanorods coated with apolipoprotein E protein Corona for drug delivery. *ACS Appl Nano Mater*. 2019;2(10):6220–6229. doi:10.1021/acsanm.9b01196
42. Dergunov AD, Vorotnikova YY. The interaction of human serum albumin in the native and fully reduced states with apolipoprotein E, serum amyloid protein and very low density lipoproteins from human plasma. *Int J Biochem*. 1994;26(7):933–942. doi:10.1016/0020-711x(94)90087-6
43. Galanakis DK. Anticoagulant albumin fragments that bind to fibrinogen/fibrin: possible implications. *Semin Thromb Hemost*. 1992;18(1):44–52. doi:10.1055/s-2007-1002409
44. Saha K, Rahimi M, Yazdani M, et al. Regulation of macrophage recognition through the interplay of nanoparticle surface functionality and protein Corona. *ACS Nano*. 2016;10(4):4421–4430. doi:10.1021/acsnano.6b00053
45. Boraschi D, Italiani P, Palomba R, et al. Nanoparticles and innate immunity: new perspectives on host defence. *Semin Immunol*. 2017;34:33–51. doi:10.1016/j.smim.2017.08.013
46. De Capua A, Palladino A, Chino M, et al. Active targeting of cancer cells by CD44 binding peptide-functionalized oil core-based nanocapsules. *RSC Adv*. 2021;11(40):24487–24499. doi:10.1039/d1ra03322k
47. Tian H, Zhang T, Qin S, et al. Enhancing the therapeutic efficacy of nanoparticles for cancer treatment using versatile targeted strategies. *J Hematol Oncol*. 2022;15(1):132. doi:10.1186/s13045-022-01320-5
48. Hoy SM. Tafasitamab: first Approval. *Drugs*. 2020;80(16):1731–1737. doi:10.1007/s40265-020-01405-w
49. Philibert P, Stoessel A, Wang W, et al. A focused antibody library for selecting scFvs expressed at high levels in the cytoplasm. *BMC Biotechnol*. 2007;7:81. doi:10.1186/1472-6750-7-81
50. Tedesco S, De Majo F, Kim J, et al. Convenience versus biological significance: are PMA-differentiated THP-1 cells a reliable substitute for blood-derived macrophages when studying in vitro polarization? *Front Pharmacol*. 2018;9:71. doi:10.3389/fphar.2018.00071
51. Cardinale D, Iacopo F, Cipolla CM. Cardiotoxicity of Anthracyclines. *Front Cardiovasc Med*. 2020;7:26. doi:10.3389/fcvm.2020.00026
52. Warga RM, Kane DA, Ho RK. Fate mapping embryonic blood in zebrafish: multi- and unipotential lineages are segregated at gastrulation. *Dev Cell*. 2009;16(5):744–755. doi:10.1016/j.devcel.2009.04.007